Experimental Aerodynamic Characteristics of an NACA 0012 Airfoil with Simulated Glaze Ice

M. B. Bragg*
Ohio State University, Columbus, Ohio

The effect of a simulated glaze-ice accretion on the aerodynamic performance of a NACA 0012 airfoil was studied experimentally. Two ice shapes were tested: one from an experimentally measured accretion, and one from an accretion predicted using a computer model given the same icing conditions. Lift, drag, and pitching moment were measured for the airfoil with both smooth and rough ice shapes. The ice shapes caused large lift and drag penalties, primarily due to large separation bubbles. Surface pressure distributions clearly showed the regions of separated flow. The aerodynamic performance of the two shapes compared well at positive, but not negative, angles of attack.

I. Introduction

MODERN computational fluid dynamics methods[1,2] are being applied to airfoils with ice accretions as part of the NASA Lewis Aircraft Icing Research Program. One of the objectives of these studies is to develop computational tools to predict the aerodynamic effect of ice accretions on aircraft. Most of the research has focused on airfoils with glaze ice where the flowfield is dominated by large separation bubbles aft of the ice horns. The correct calculation of these bubbles is critical to the accuracy of the computer model.

Detailed baseline data are needed on airfoils with glaze ice to help develop these computer codes. Although several studies[3-9] have reported experimental measurements of the effect of ice on overall airfoil performance, little detailed work has been done. To supply these data, Bragg and his co-workers[10-13] studied the effect of a simulated ice shape on a NACA 0012 airfoil. References 10, 12, and 13 give a detailed look at the split film velocity profiles in the separation bubble. Pressure distribution and lift, drag, and moment data were reported in Refs. 11 and 13.

This paper presents the experimental results for lift, drag, and pitching moment for the NACA 0012 airfoil with simulated glaze ice. The initial experiments[10-12] were conducted with a simulation of the experimentally measured ice shape. Aerodynamic measurements on a computer-generated ice shape[13] are presented and compared to the earlier ice shape data. This paper summarizes the effect on the integrated airfoil performance of the two glaze-ice shapes from Refs. 11-13. These data are currently being used to develop and validate the computational results.

II. Experimental Procedure

Apparatus

These tests were conducted in Ohio State University's subsonic wind tunnel located at the Aeronautical and Astronautical Research Laboratory. The tunnel is of conventional design with a 3×5 ft test section, 8 ft in length. The tunnel operates at speeds of up to 220 ft/s and Reynolds numbers up to 1.3×10^6/ft. The tunnel is of open return type and uses four turbulence screens and honeycomb in the settling chamber to reduce the tunnel turbulence. Tunnel speed, Reynolds number, and Mach number are provided through facility pressure transducers.

A specially built NACA 0012 airfoil model was used for these tests. The model has a 21 in. chord, which was cut from mahogany using a numerical control machine and laminated together to form the 39 in. span. A unique feature of this model is its interchangeable leading edges. Past experiences using simulated ice on airfoils has identified a problem with the proper placement of an ice shape over a clean leading edge. To avoid this problem, the current model has the ice shape as an integral part of the first 15% of the model. In this way, the first 15% of the model was attached precisely to the main model section and the exact airfoil plus ice shape geometry accurately known.

Experience with earlier simulated models[10] demonstrated the need for a very dense placement of surface pressure taps. The current model was internally tapped with approximately 90 surface pressure plots. The upper surface was instrumented with a tap every 1% (0.21 in.) surface length back to the 40% chord station. Another 40 taps were located around the rest of the airfoil on the model centerline. Eight taps were located spanwise at the 5% station and were used as an indication of the two-dimensionality of the flow.

Two different iced leading edges were tested on the NACA 0012 model. Both were intended to represent a 5 min glaze-ice accretion with an angle of attack of 4 deg and the freestream velocity of 130 mph. The icing conditions were a volume median diameter droplet of 20 μm, liquid water content of 2.1 g/m^3, and a temperature of 18°F. The first leading-edge ice shape is referred to in this paper as the simulated shape. The simulated shape is a simple approximation of the ice accretion measured in the NASA Icing Research Tunnel at these conditions. It was originally intended to be a simple, but fairly representative, glaze-ice accretion shape to be used to gather information for computer code validation. This is the ice shape used in the previous studies. The cross section of the simulated shape and the NASA Lewis measured shape are shown in Fig. 1. The simulated shape has a smooth surface and contains 19 pressure taps ahead of the 5% chord station. The second iced leading edge for the NACA 0012 airfoil model is referred to in this paper as the LEWICE shape. It is a shape predicted by the LEWICE computer code[14,15] for these icing conditions. As can be seen in Fig. 1, the shape is similar to the measured and simulated shapes. This model was built from the computer-generated coordinates and was pressure tapped with 17 taps ahead of the 5% chord location. Both models were constructed of fiberglass with a foam core.

For those tests where the roughness of the ice was simulated, a sand grain type of roughness was added to the glaze-ice simulation. Roughness was applied only to the ice surface from an $x/c = 0.085$ on the lower surface forward around the ice shape and terminating at $x/c = 0.015$ on the upper surface. Sandpaper with a cloth backing was applied to the model with

Received Feb. 20, 1988; revision received June 10, 1988.

*Associate Professor, Department of Aeronautical and Astronautical Engineering. Senior Member AIAA.

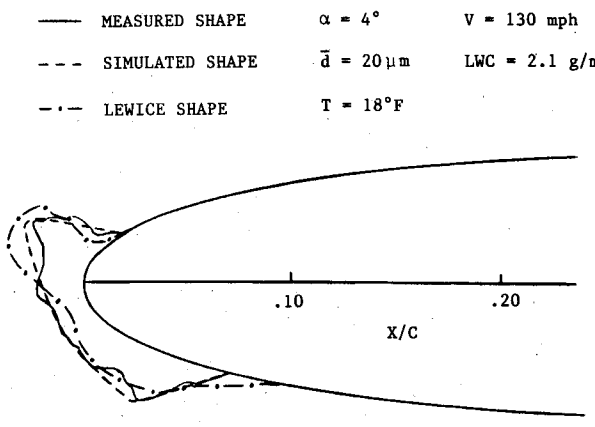

Fig. 1 Measured, simulated, and LEWICE ice shapes.

adhesive to simulate the roughness. Holes were placed in the sandpaper for each surface pressure port covered and were carefully sealed to prevent any leakage between the airfoil surface and sandpaper backing. Two roughness sizes were used: a number 60 grit paper that has a nominal roughness element size of 0.012 in., roughness height-to-chord ratio $k/c =$ 0.00057, and a number 36 grit paper where $k/c = 0.0011$. Only data from the larger, 36 grit roughness are presented here.

Standard tunnel instrumentation was used for this test. Pressure measurements were made using a Scanivalve system. Two Scanivalves capable of measuring 48 pressures each were used. The scanivalves were connected in series sharing one pressure transducer to reduce calibration time and improve the accuracy of the measurements. No cutoff valves were used for this test. A single traversing total pressure probe was used to measure the airfoil wake. The probe was located approximately one chord length downstream of the model trailing edge.

Data Acquisition and Reduction

Data acquisition and reduction were accomplished primarily on the Laboratory's Harris H800 computer. Several analog-to-digital systems are available at the Laboratory; a medium-speed (8 kHz) RTP system with 12 bit resolution was used for these tests. The system is operated through a CRT terminal with disk and tape storage available as well as printed and plotted hardcopy. At the completion of a run, raw voltages and all system configuration and calibration data are written to magnetic tape. The terminal operator then has the option to reduce the data online or to wait to reduce at a later time.

For these tests, airfoil lift and moment coefficients were determined from the integrated surface pressure measurements. The airfoil drag coefficient was determined by an integration of the wake momentum deficit measured by the wake total pressure probe.

III. Results and Discussion

Clean Model

Initial tests were conducted on the NACA 0012 model without the ice shape. This is referred to as the clean configuration. Due to the slight seam in the model at the 15% chord location where the leading-edge section meets the main model body, there was some question regarding its effect on the boundary-layer transition location. To remove this question and for ease in comparing these measurements to the computational results, tests also were run with the boundary layer tripped at the 5% chord location on the upper and lower surfaces. The trip strip used was carborundum grit, 0.009 in. in size, attached to the model using double-sided tape. The trip was approximately 0.25 in. in the chordwise direction with the back edge at the 0.05 x/c location. Only results from measurements at positive angles of attack are shown for the clean

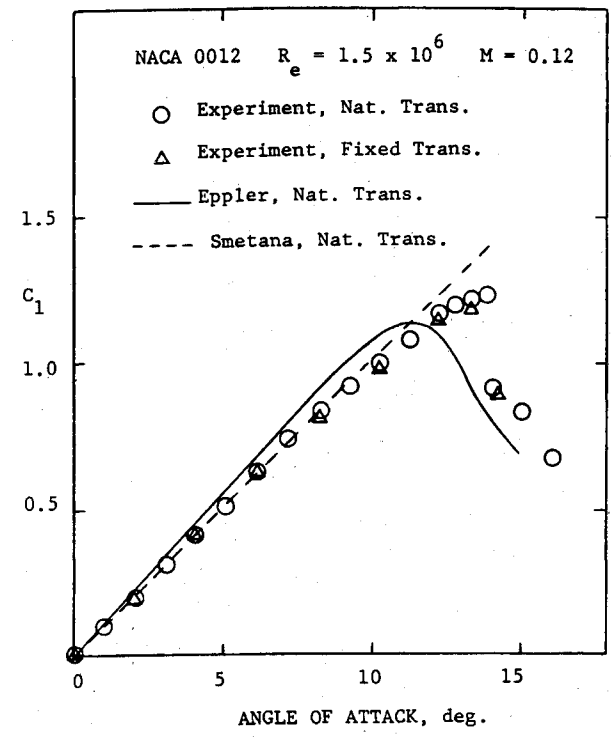

Fig. 2 Measured and predicted lift with natural and fixed transition (clean configuration).

airfoil, with or without trip. Negative angles to stall were tested, but were essentially identical to those at positive angles of attack. All data presented here have been corrected for tunnel wall effects by applying the correction method of Rae and Pope.[16]

In Fig. 2, the lift coefficient as a function of angle of attack for the clean model is shown. Presented are the data for a Reynolds number of 1.5×10^6 and Mach number of 0.12. Also shown are the theoretical predictions from the airfoil analysis codes of Eppler and Somers[17] and Smetana et al.[18] The lift curve slope compares well to the results of Smetana, since this code iterates on the displacements thickness to include the decambering of the airfoil due to boundary-layer growth. Eppler merely assumes a lift curve slope of 2π/rad and thus overpredicts these data. The Eppler code does contain a simple $C_{\ell_{max}}$ prediction that predicts a $C_{\ell_{max}}$ of approximately 1.12 at 1.5×10^6 Reynolds number compared to the measured value of 1.22. Tests were also run at a Reynolds number of 0.9 and 2.0×10^6 with little effect on the lift.

The measured drag performance of this airfoil is presented in Fig. 3. Here, the experiment, as well as the theories of Refs. 17 and 18, are shown with natural and fixed transitions. Both theories show more of a drag bucket than is reflected in the experiment, although some bucket is seen in the data. At zero angle of attack and with natural transition, the experimental data have a drag coefficient of 0.0075, with 0.0070 and 0.0067 predicted by Refs. 17 and 18, respectively. This is due to early transition on the wind-tunnel model since the data with the boundary layer tripped compare very well to theory. With the transition fixed at the 5% station, the measured drag coefficient rises to 0.0106, while the theories are only 0.0002 or 0.0003 higher. The comparison remains excellent until the theories fail to predict the large drag rise associated with separation at high angle of attack. Experimental and theoretical results also were obtained at 0.9 and 2.0×10^6 Reynolds number. The drag coefficient increased with decreasing Reynolds number, as expected.

Pitching moment data were taken and compared reasonably well to theory. Little effect of early transition was seen in these data.

Typical pressure distributions are shown in Fig. 4. Here the measured pressures are compared to those predicted by the Smetana code. Comparisons are made at the matched lift coefficient, since the experimental angle of attack contains the wall boundary corrections. The experimental data are for uncorrected angles of attack of 2 and 6 deg. The comparisons are excellent with only some small deviation near the 15% chord location. This is probably due to the slight discontinuity where the model leading edge joins the main element. Note that with the very dense measured pressures near the leading edge, every symbol represents a measured pressure. The measured minimum pressure coefficient was in good agreement to the theory. Changes in C_p with Reynolds number and with the boundary-layer trip were small, as expected.

Model with Glaze Ice

An airfoil with a large leading-edge glaze-ice shape experiences a large region of flow separation aft of the ice horns (Fig. 5). The flow first accelerates around the ice horns and then experiences a large adverse pressure gradient as it decelerates aft of the horn to join the original airfoil contour. It then separates near the trip of the ice horn and, at low angles of attack, reattaches downstream forming a separation bubble. These separation bubbles act to increase airfoil drag and burst at a large angle of attack, causing flow separation on the entire upper surface and a large loss in $C_{l_{max}}$.

In Fig. 6, pressures for 0, 2, and 4 deg angle of attack are shown for the airfoil with simulated glaze ice. The circles represent the pressures measured at zero angle of attack. Here the lower- and upper-surface separation zones are identified as the regions of relatively constant pressure at C_p of approximately -0.9 and -0.7, respectively. As the angle of attack is increased, these constant-pressure zones occur at decreasing pressures for the upper-surface separation and increasing pressures for the lower. Note also that at $\alpha = 0$ deg the upper-surface separation occurs at a higher pressure than the lower-surface separation. At 2 and 4 deg, this is reversed with the upper-surface separation zone occurring at a lower pressure level.

In Fig. 7, the pressure distributions for angles of attack of 4, 6, and 8 deg are shown. Here, as the airfoil begins to approach stall, the upper-surface separation bubble grows rapidly in length and the constant-pressure zone occurs at higher pressures. Remember that the airfoil stalls at approximately 7 deg angle of attack. As the angle of attack increases, the trailing-edge pressure is seen to fall, as do the pressures on the entire aft portion of the airfoil. At 8 deg angle of attack, the airfoil has stalled; the scatter in the leading-edge pressures measured at the upper surface is an indication of the unsteadiness of the flow in this region.

Figures 8 and 9 show the lift performance of the clean NACA 0012 and the airfoil with both ice shapes, smooth and rough. At positive angles of attack (Fig. 8), a large lift penalty is seen at angles of attack above 6 deg. The maximum lift coefficient is reduced by more than 50% for both ice shapes, with the simulated shape having a slightly lower maximum lift than the

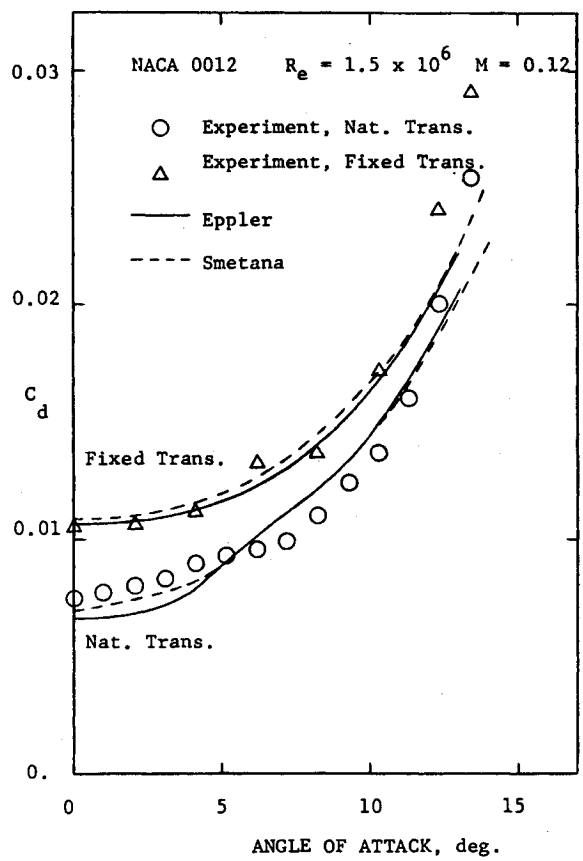

Fig. 3 Measured and predicted drag with natural and fixed transition (clean configuration).

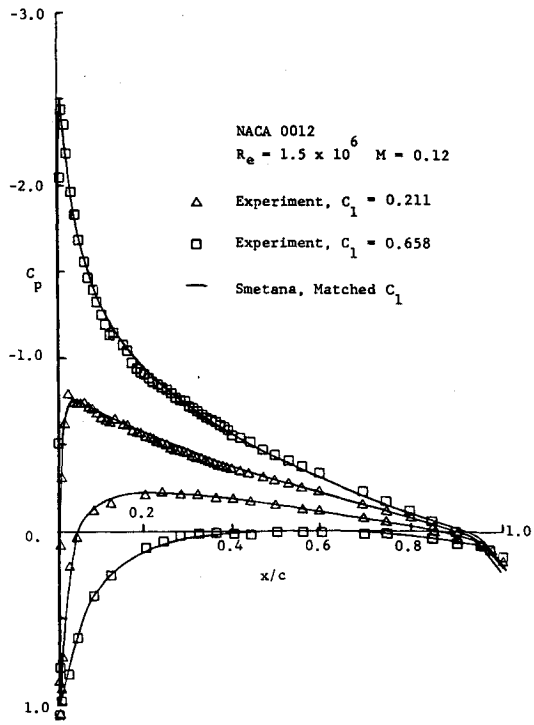

Fig. 4 Measured and predicted surface pressures at two angles of attack (clean configuration).

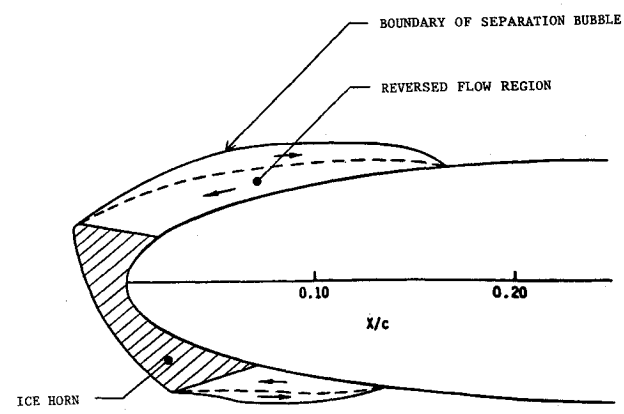

Fig. 5 Separation bubbles due to the glaze-ice shape.

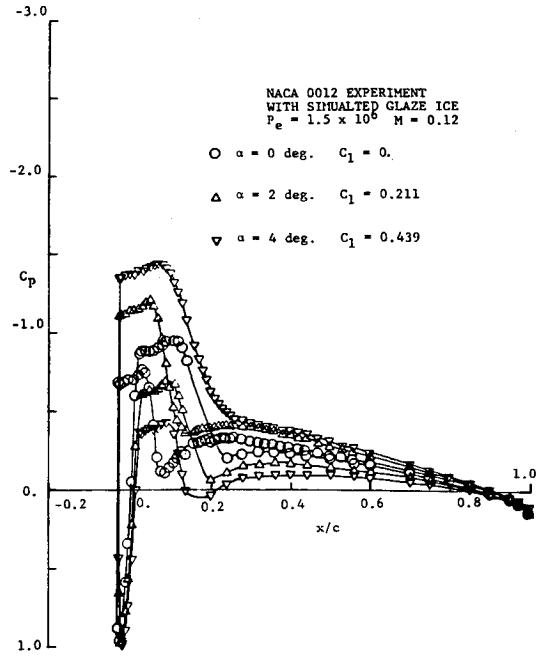

Fig. 6 Measured surface pressures with simulated ice at low angles of attack.

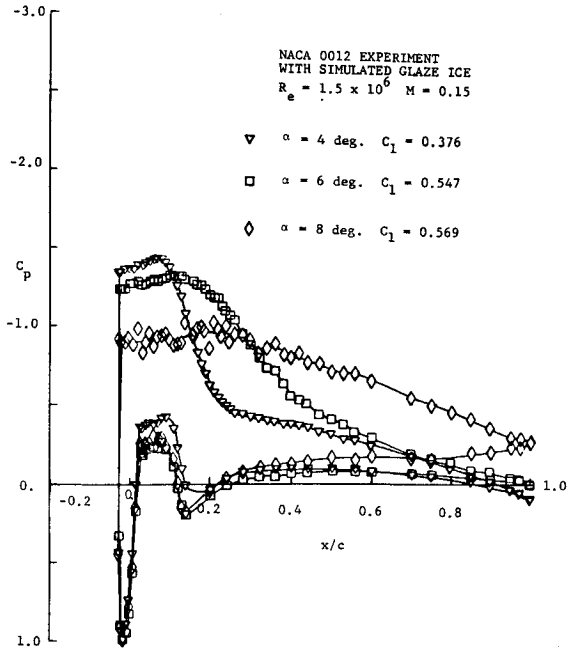

Fig. 7 Measured surface pressures with simulated ice at high angles of attack.

LEWICE shape. Both ice shapes stall at approximately 6 deg angle of attack. Note that, for both ice shapes, the surface roughness has little effect on the lift since the effect on bubble separation and reattachment are small. At positive angles of attack, the LEWICE and the simulated ice shape have similar performance, although the LEWICE upper horn is somewhat larger (Fig. 1).

The lift performance at negative angles of attack is shown in Fig. 9. Here, the aerodyamics are greatly affected by the separation bubble on the lower surface created by the lower-surface ice horn. From Fig. 1, these are seen to be somewhat different for the two ice shapes. The LEWICE shape has a very rounded lower ice horn, while the simulated shape more accurately reproduces the very sharp horn seen in the actual

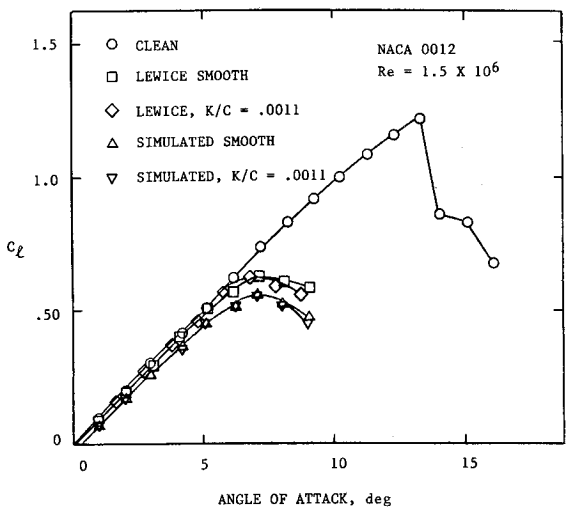

Fig. 8 Lift performance clean and with simulated and LEWICE ice shapes at positive angles of attack.

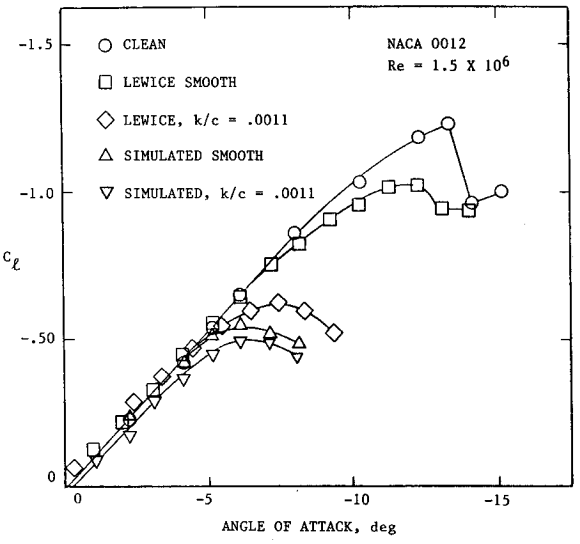

Fig. 9 Lift performance clean and with simulated and LEWICE ice shapes at negative angles of attack.

measured ice shape. The effect of these differences is seen clearly in Fig. 9. The simulated shape, either smooth and rough, causes a large reduction in maximum lift of approximately the same magnitude as that at positive angles. The smooth LEWICE shape suffers a large lift loss when roughness is added due to the increase in the size of the lower-surface separation bubble. With roughness, the LEWICE shape has about the same lift as the simulated shape.

While no flow visualization has been done on the LEWICE shape, much can be learned by examining the pressure distribution. In Fig. 10, the pressure coefficients are shown for both smooth ice shapes at 4 deg angle of attack. Note the upper-surface bubble is seen as the constant-pressure region around a pressure coefficient of −1.4. For both ice shapes, the constant-pressure regions and, therefore, the upper-surface bubbles are very similar. At −4 deg angle of attack (Fig. 11), the comparison is much different. Note that, at −4 deg, the lower-surface appears on the top of the pressure coefficient curve corresponding to negative values. For the smooth simulated shape, a large lower-surface bubble is seen as the constant-pressure region with a pressure coefficient of approximately −1.2. Adding roughness has little effect on the simulated shape and is therefore not shown. However, with the smooth LEWICE shape, the pressure coefficient around the

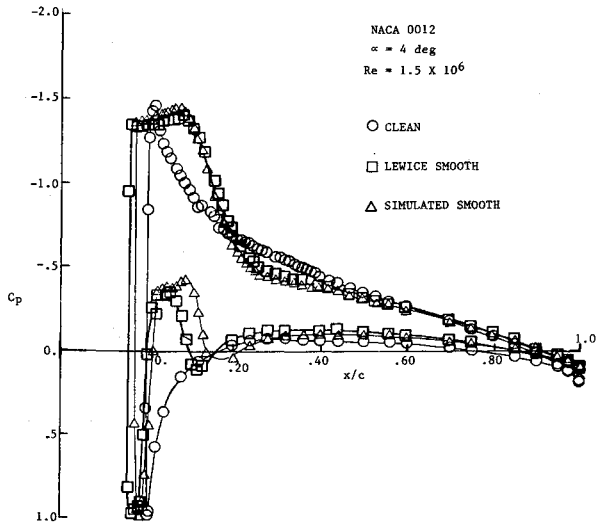

Fig. 10 Pressure distribution clean and with simulated and LEWICE ice shapes at 4 deg angle of attack.

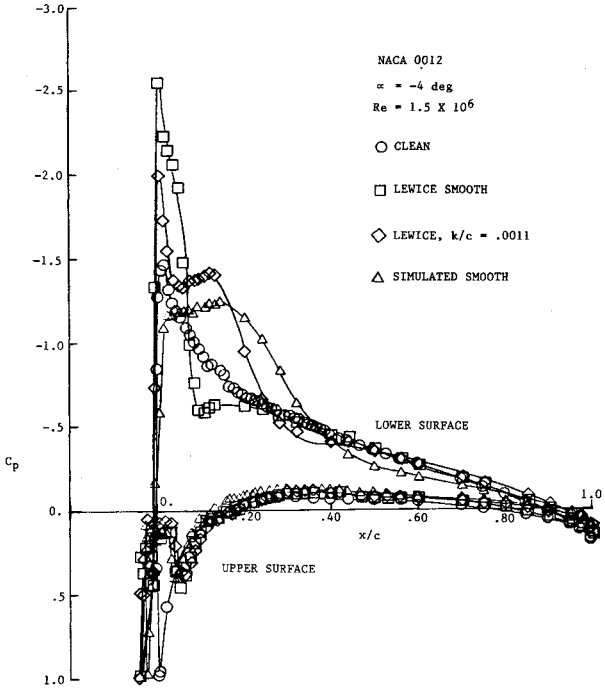

Fig. 11 Pressure distribution clean and with simulated and LEWICE ice shapes at −4 deg angle of attack.

lower horn spikes to −2.5 and no large separation is seen. Adding roughness to the LEWICE shape causes a large separation bubble to form aft of the lower-surface ice horn, greatly changing the surface pressures. Here, although the spike remains, it is followed by a large constant-pressure region (separation bubble) at a pressure coefficient of −1.4. Adding roughness greatly improved the comparison of the LEWICE and simulated shapes by forming the large lower-surface separation bubble.

The importance of correctly predicting the ice horns when using computer-generated ice shapes is demonstrated by the difference between the positive and negative angle of attack lift performance seen here. As an additional comment, the performance of the LEWICE shape at negative angles of attack is similar to that of a rime ice shape where roughness usually does significantly affect the measured aerodynamic performance, even though the aerodynamic process may be different.

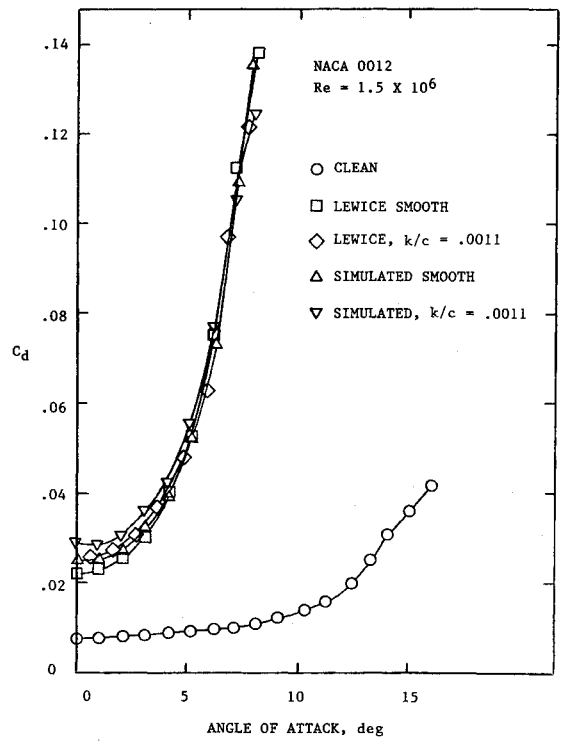

Fig. 12 Drag performance clean and with simulated and LEWICE ice shapes at positive angles of attack.

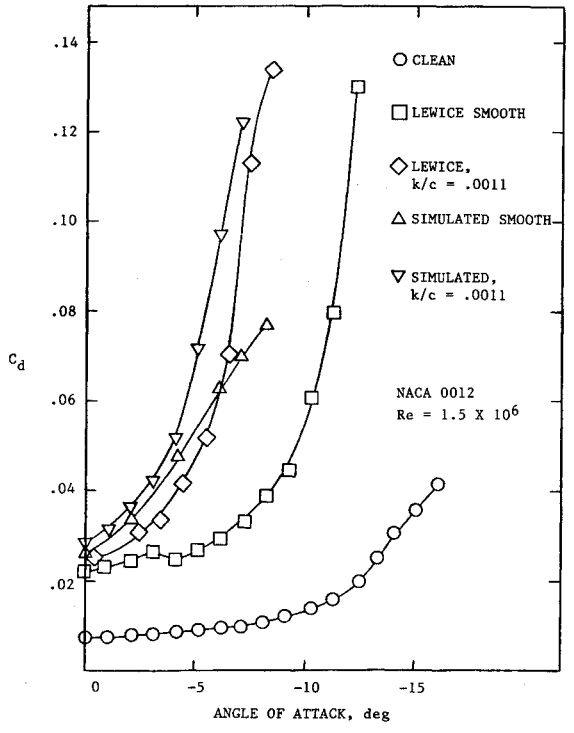

Fig. 13 Drag performance clean and with simulated and LEWICE ice shapes at negative angles of attack.

Figures 12 and 13 show the drag performance of the airfoil and correspond to Figs. 8 and 9. The same trends that were seen in Figs. 8 and 9 are also clearly evident here. At positive angles of attack (Fig. 12), the drag for the simulated and LEWICE shapes is almost identical with the simulated shape, only slightly higher. Roughness does increase the drag somewhat at low angles of attack, but the increment is small compared with the effect of the smooth ice alone. The airfoil drag at negative angles of attack is shown in Fig. 13. While both ice shapes

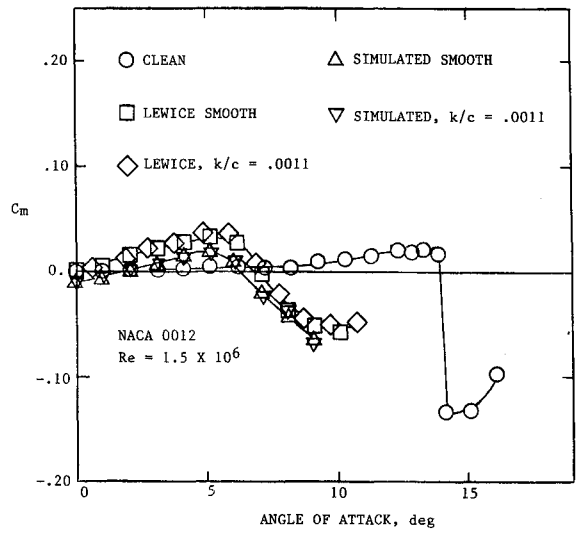

Fig. 14 Pitching moment about the quarter-chord clean and with simulated and LEWICE ice shapes at positive angles of attack.

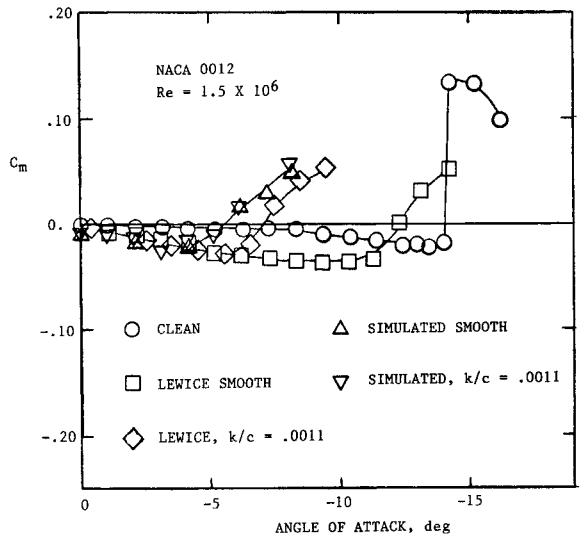

Fig. 15 Pitching moment about the quarter-chord clean and with simulated and LEWICE ice shapes at negative angles of attack.

greatly increase the drag, the LEWICE shape is seen to be affected more by the roughness. As explained earlier, the smooth LEWICE shape has a less significant aerodynamic penalty than when roughness is added, due to the more rounded lower-surface ice horn. As with the lift, the rough LEWICE shape has a drag level similar to the rough simulated shape; however, the smooth LEWICE shape has much less drag than the simulated shape. Roughness has some effect on the simulated shape, particularly at high, negative angles of attack where the roughness reduces lift and increases the drag.

The pitching moment data about the airfoil quarter chord are shown in Figs. 14 and 15. Figure 14 is for positive angles of attack and, as expected from the lift and drag data, the two ice shapes compare very well. For the clean, symmetric airfoil, the pitching moment is essentially zero until boundary-layer growth, and then separation, cause a nose-up moment and then a larger nose-down moment as the airfoil stalls at large angles of attack. The addition of the ice shape changes the airfoil camber distribution and boundary-layer characteristics affecting the pitching moment. The pitching moment for the iced airfoils has an increasing nose-up moment until at approximately 7 deg angle of attack the airfoil stalls, producing a nose-down moment. At negative angles of attack (Fig. 15), the pitching moment coefficient values are of opposite sign for the clean case. With the ice shapes, the trends are as expected from the lift performance. A large influence of surface roughness on the LEWICE shape is seen with only the rough LEWICE shape having pitching moments similar to the simulated shape.

IV. Summary

This experimental study documents the aerodynamics of a NACA 0012 airfoil with glaze-ice simulations. A computer-predicted glaze-ice shape was tested on the NACA 0012 airfoil and compared to results on a simulation of a measured shape. Both ice shapes severely degraded the airfoil performance, reducing lift and increasing the drag. The aerodynamics of the airfoil with the two ice shapes is very similar at positive angles of attack, but only the rough ice shapes compare well at negative angles of attack. This difference is due to the LEWICE compuer code underpredicting the lower-surface glaze-ice horn. These data provide an initial look at how well an ice shape must be predicted to have aerodynamic penalties similar to an actual accreted ice shape.

Acknowledgment

This work was supported by a grant from NASA Lewis Research Center. The author wishes to thank Dr. R. J. Shaw and Mr. M. G. Potapczuk of NASA Lewis for their support of this effort.

References

[1]Potapczuk, M. G., "Navier-Stokes Computations for a NACA 0012 Airfoil with Leading Edge Ice," AIAA Paper 87-0101, Jan. 1987.

[2]Cebeci, T., "The Calculation of Flow Over Iced Airfoils," AIAA Paper 88-0101, Jan. 1988.

[3]Gray, V. H. and Von Glahn, U. H., "Effects of Ice and Frost Formations on Drag of NACA 65-212 Airfoil for Various Modes of Thermal Ice Protection," NACA TN-2962, 1953.

[4]Gray, V. H. and Von Glahn, U. H., "Aerodynamic Effects Caused by Icing of an Unswept NACA 65A004 Airfoil," NACA TN-4151, 1957.

[5]Bragg, M. B., Zaguli, R. J., and Gregorek, G. M., "Wind Tunnel Evaluation of Airfoil Performance Using Simulated Ice Shapes," NASA CR-167960, 1982.

[6]Bragg, M. B. and Gregorek, G. M., "Wind Tunnel Investigation of Airfoil Performance Degradation Due to Icing," AIAA Paper 82-0582, March 1982.

[7]Ingelman-Sundberg, M., Trunov, O. K., and Ivaniko, A., "Methods for Prediction of the Influence of Ice on Aircraft Flying Characteristics," *Joint Report of the 6th Meeting of Swedish-Soviet Working Group on Flight Safety,* NASA Lewis Research Center, 1977.

[8]Flemming, R. J. and Lednicer, D. A., "High Speed Ice Accretion on Rotor Airfoils," NASA CR-3910, Aug. 1985.

[9]Bragg, M. B., Gregorek, G. M., and Lee, J. D., "Airfoil Aerodynamics in Icing Conditions," *Journal of Aircraft,* Vol. 23, Jan. 1986, pp. 76–81.

[10]Bragg, M. B. and Coirier, W. J., "Detailed Measurements of the Flowfield in the Vicinity of an Airfoil with Glaze Ice," AIAA Paper 85-0409, Jan. 1985.

[11]Bragg, M. B. and Coirier, W. J., "Aerodynamic Measurements of an Airfoil with Simulated Glaze Ice," AIAA Paper 86-0484, Jan. 1986.

[12]Bragg, M. B. and Spring, S. A., "An Experimental Study of the Flow Field About an Airfoil with Glaze Ice," AIAA Paper 87-0100, Jan. 1987.

[13]Bragg, M. B. and Khodadoust, A., "Experimental Measurements in a Large Separation Bubble Due to a Simulated Glaze Ice Shape," AIAA Paper 88-0116, Jan. 1988.

[14]Ruff, G. A., "Development of an Analytical Ice Accretion Prediction Method," AIAA Paper 87-0098, Jan. 1987.

[15]Berkowitz, B., private communication, Cleveland, OH, Aug. 28, 1987.

[16]Rae, W. H., Jr. and Pope, A., *Low-Speed Wind Tunnel Testing,* 2nd ed., Wiley, New York, 1984.

[17]Eppler, R. and Somers, D. M., "A Computer Program for the Design and Analysis of Low-Speed Airfoils," NASA TM-80210, Aug. 1980.

[18]Smetana, F. O., Summey, D. C., Smith, N. S., and Carden, R. K., "Light Aircraft Lift, Drag, and Moment Prediction—A Review and Analysis," NASA CR-2523, May 1975.